

Shock Tube Measurements of Branched Alkane Ignition Times and OH Concentration Time Histories

M. A. OEHLSCHLAEGER, D. F. DAVIDSON, J. T. HERBON, R. K. HANSON

Mechanical Engineering Department, Stanford University, Stanford, California 94305-3032

Received 15 May 2003; accepted 12 September 2003

DOI 10.1002/kin.10173

ABSTRACT: Ignition times and hydroxyl (OH) radical concentration time histories were measured behind reflected shock waves during the oxidation of three branched alkanes: iso-butane (2-methylpropane), iso-pentane (2-methylbutane), and iso-octane (2,2,4-trimethylpentane). Initial reflected shock conditions ranged from 1177 to 2009 K and 1.10 to 12.58 atm with dilute fuel/O₂/Ar mixtures varying in fuel concentration from 100 ppm to 1.25% and in equivalence ratio from 0.25 to 2. Ignition times were measured using endwall CH emission and OH concentrations were measured using narrow-linewidth ring-dye laser absorption of the R₁(5) line of the OH A-X (0,0) band at 306.7 nm. The ignition times and OH concentration time histories were compared to modeled predictions of seven branched alkane oxidation mechanisms currently available in the literature and the implications of these comparisons are discussed. These data provide a unique database for the validation of detailed hydrocarbon oxidation mechanisms of propulsion related fuels. © 2003 Wiley Periodicals, Inc. *Int J Chem Kinet* 36: 67–78, 2004

INTRODUCTION

Branched alkanes are important components of practical fuels. Despite their relatively high concentrations in practical fuels (~30% of gasoline), the ignition times of branched alkanes have not been extensively studied, and previous shock tube studies show large scatter in the data [1–5]. Increasing the ratio of branched alkanes (high research octane numbers—RON) to nor-

mal alkanes (low RON) in a fuel is well known to reduce engine knock (auto-ignition). The propensity for branched alkanes to act as inhibitors of auto-ignition is related to the strong radical scavenging that occurs during their oxidation, which delays the ignition times of branched alkanes relative to their straight chain counterparts.

During hydrocarbon oxidation the radical pool controls the ignition process, and understanding of this radical pool via measurement is crucial for developing combustion models. At present most models target shock tube ignition times, flame speeds, and/or stable species measurements. Detailed information about the transient radical pool (OH, CH₃, HCO, H, etc.) will allow refinement to the detailed chemistry models that

Correspondence to: Matt Oehlschlaeger; e-mail: moehlsch@stanford.edu.

Contract grant sponsor: Army Research Office.

Contract grant number: DAAD 19-01-1-0597.

© 2003 Wiley Periodicals, Inc.

are used to calculate radical time histories, which in turn will allow better predictions of the global kinetic parameters needed for engineering applications.

The motivation for the current study arises from the desire to provide target data for simple fuels that are components of or analogs to larger molecules that exist in gasoline and diesel fuel. Here we present ignition time and OH concentration time history data measured during the oxidation of iso-butane, iso-pentane, and iso-octane behind reflected shock waves. Hydrocarbon fuels do not actually contain significant amounts of iso-octane or iso-butane, though they do contain significant amounts of iso-pentane. As the simplest branched alkane, iso-butane is the first step towards building an understanding of the role of branched alkanes in oxidation. It is especially important to understand the contribution of branched alkane decomposition products to the radical suppression process during oxidation.

In this work we compare the new ignition time data and OH concentration time histories to calculations based on different branched alkane reaction mechanisms; none of these mechanisms have been directly validated using transient radical pool data, as none were available. The smaller branched alkanes, iso-butane and iso-pentane, have not been modeled as extensively as iso-octane, a primary reference fuel of great importance. A mechanism from Bounaceur and Battin-Leclerc [6] (177 species and 927 reactions) and a mechanism from Wang et al. [7] (386 species and 1896 reactions) will be examined for the modeling of the oxidation of iso-butane; and another mechanism from Bounaceur and Battin-Leclerc [6] (187 species and 976 reactions) will be examined for iso-pentane oxidation. The mechanisms from Bounaceur and Battin-Leclerc were automatically generated via computer, much like previous work from this group [8,9] using reaction classes and a lumped kinetic scheme that includes submechanisms from earlier work on methane and ethane [10]. These mechanisms although not published are easily obtained by contacting the EXGAS group in Nancy, France [6]. The Wang et al. mechanism was targeted to describe the low temperature oxidation (600–900 K) of neo-pentane but includes the necessary reactions to describe the oxidation of iso-butane at the temperatures of our experiments.

Mechanisms that will be examined for the oxidation of iso-octane are the following: Curran et al. [11], Davis and Law [12], Pitsch et al. [13], and Ranzi et al. [14]. These iso-octane reaction mechanisms vary considerably in size. The Curran et al. mechanism contains 990 species and 4060 reactions and represents a sub-mechanism of the recent version of the full LLNL reference fuel mechanism which models *n*-heptane and

iso-octane oxidation [11]. The Davis and Law mechanism (69 species and 406 reactions) was formed from adding iso-octane-specific reactions to the Held et al. [15] mechanism for *n*-heptane. The Pitsch et al. mechanism was developed for full engine calculations and contains only 47 species and 134 reactions. The Ranzi et al. mechanism (145 species and 2500 reactions) was developed much like the EXGAS mechanisms, using reaction classes and a lumped kinetic scheme, and includes submechanisms from their earlier work on *n*-heptane [16].

The ability of all these mechanisms to predict ignition times and OH concentration time histories are investigated in the current study. Contribution and sensitivity analysis is also presented in order to give kinetic implications for these measurements and to provide direction for the future development of branched alkane oxidation models.

This work continues on the path of previous work from our laboratory that seeks to improve the database of kinetic targets used for modeling hydrocarbon fuel oxidation. Recent work has included the measurement of ignition times and OH and C₂H₄ concentration time histories for four *n*-alkanes: propane, *n*-butane, *n*-heptane, and *n*-decane [17,18].

EXPERIMENTAL METHOD

Experiments were performed in two different high-purity, helium-driven, stainless steel shock tubes. One shock tube is 15.24 cm in diameter and has a 10.51 m long test section; the other is 14.13 cm in diameter and has an 8.54-m-long test section; both test sections are pumped down between experiments with turbo pumps with ultimate pressures on the order of 10⁻⁷ Torr. Shock velocities were extrapolated to the endwall from four incident shock wave velocity measurements made with piezo pressure transducers over the last 1.5 m of the shock tube. The pre-shock initial mixture pressure was measured using a high-accuracy Baratron pressure transducer. Reflected shock conditions were calculated using standard normal-shock relations and thermochemical data taken from the Sandia thermodynamic database. Thermochemical data for iso-octane was taken from Burcat and McBride [19]. Uncertainty in the reflected shock temperature is estimated to be 10 K, primarily due to uncertainty in the shock velocity measurement. The temperature uncertainty results in about a 10% uncertainty in the measured ignition times. Mixtures were made in a stainless steel chamber with a built-in stirring system. Research grade Ar (99.999%) and O₂ (99.993%) were used and all fuels were from Aldrich: 99+% iso-butane, 99.5+% iso-pentane,

and 99.7+% iso-octane. The initial reflected shock conditions for these experiments was 1177–2009 K and 1.10–12.58 atm, with fuel mole fractions of 100 ppm to 1.25%, and equivalence ratios, Φ , from 0.25 to 2.0.

Ignition times were measured using CH emission viewed from the endwall, since the measured ignition time at points away from the endwall may be artificially decreased by the combustion wave that propagates down the shock tube after ignition occurs at the endwall. CH emission was measured with a fast (1.6 μ s risetime) silicon photodetector and a 10 nm bandpass filter centered at 431 nm. For greater detail about the efforts made to minimize experimental uncertainty in ignition time data taken in our facilities see Horning et al. [20]. The ignition time is defined as the time between shock arrival at the endwall, determined by the incident shock velocity, and the extrapolation of the maximum CH emission slope to zero value (see Fig. 1).

OH concentration time histories were measured by passing a narrow-linewidth CW UV laser beam (306.7 nm) across the shock tube at a location 2 cm from the endwall. The well characterized $R_1(5)$ line of the OH $A^2 \Sigma^+ - X^2 \Pi(0,0)$ band was used for absorption. The UV-beam was created by pumping a ring-dye laser to create red light at 613.4 nm, and intra-cavity doubling of this light, with a AD*A crystal, produced light at 306.7 nm. The uv-beam was detected with two Si photodetectors, before and after passing through the absorbing gas in the shock tube. Absolute OH concentrations were calculated using the Beer-Lambert relation. We estimate uncertainties in the resultant OH mole fraction for these measurements at 5%; the

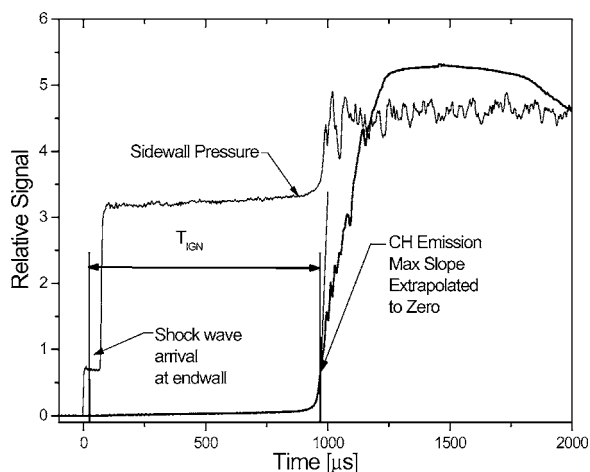


Figure 1 Iso-octane ignition: CH emission profile and PZT pressure trace. Initial shock conditions: 0.25% iso-octane, 6.25% O₂, 1269 K, 8.07 atm. Ignition time is 952 μ s.

largest source of uncertainty stems from the OH oscillator strength ($\pm 2\%$) and the collisional-broadening parameter. For details about this measurement, see past work from our laboratory, e.g., Wooldridge et al. [21] and Herbon et al. [22].

Off-line (nonresonant) absorption was observed during the iso-octane experiments but not during iso-butane or iso-pentane experiments. This absorption is likely from intermediate olefins and was also detected during previous experiments with JP-10 [23]. The interference absorption was subtracted from the on-line absorption to recover corrected OH concentration time histories. Example on-line and off-line absorption traces are shown in Fig. 2. The large signal-to-noise ratio and high sensitivity of this diagnostic permit measurement of ppm level OH with μ s time resolution.

EXPERIMENTAL RESULTS AND DISCUSSION

Ignition Time Data

Ignition time data were obtained in 187 total experiments (presented in Table I); 58 for iso-butane, 34 for iso-pentane, and 95 for iso-octane. These ignition times have been correlated using a regression analysis to provide expressions for ignition time as a function of temperature, pressure, O₂ mole fraction, and equivalence ratio. These parameters (T , P , X_{O_2} , and Φ) were all varied individually during the experimental procedure to determine their respective effects on ignition time. The following correlations for

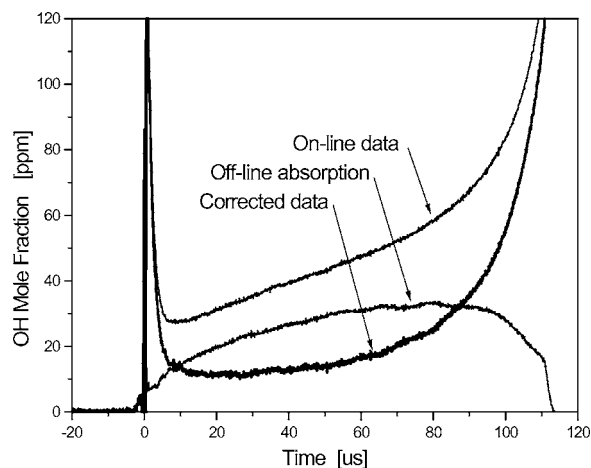


Figure 2 OH absorption: on-line, off-line, and corrected profile. Initial shock conditions: 1.0% iso-octane, 6.25% O₂, 1656 K, 1.34 atm. Reflected shock arrival, $t = 0$; ignition, $t = 116 \mu$ s.

Table I Branched Alkane Ignition Times

Fuel (%)	O ₂ (%)	T ₅ (K)	P ₅ (atm)	τ _{ign} (μs)
Iso-butane				
0.01	0.065	1526	1.53	1114
		1571	1.60	754
		1616	1.52	474
		1679	1.43	265
		1737	1.43	168
		1864	1.33	72
0.05	0.325	1444	1.59	1731
		1546	1.58	507
		1630	1.49	195
		1703	1.40	115
		1442	2.71	1338
		1540	2.78	512
		1603	2.70	224
		1625	2.54	184
		1723	2.47	75
		1765	2.00	62
		1406	5.53	1515
		1545	5.61	338
		1577	5.03	231
		1750	4.78	45
0.1	0.65	1404	11.12	1281
		1473	10.69	554
		1542	10.32	305
		1607	12.58	144
		1684	9.94	73
		1411	1.55	1807
		1488	1.57	741
		1491	1.50	639
		1522	1.56	458
		1593	1.46	246
0.125	3.25	1720	1.41	72
		1291	1.67	1404
		1341	1.63	672
		1390	1.56	329
0.25	3.25	1474	1.51	113
		1339	1.69	1135
		1402	1.62	493
		1488	1.58	166
0.5	3.25	1541	1.47	96
		1366	1.61	1475
		1426	1.55	694
		1520	1.49	258
1.0	3.25	1646	1.46	77
		1461	1.52	1159
		1566	1.45	450
		1569	1.47	453
1.0	6.5	1681	1.35	155
		1346	1.58	1162
		1351	1.56	1096
		1379	1.55	675
		1383	1.56	764
		1403	1.53	634
		1434	1.56	381

Continued

Table I Continued

Fuel (%)	O ₂ (%)	T ₅ (K)	P ₅ (atm)	τ _{ign} (μs)
		1445	1.49	379
		1455	1.54	324
		1545	1.49	118
		1555	1.44	120
		1565	1.48	118
Iso-pentane				
0.025	0.8	1300	1.64	1679
		1399	1.74	342
		1431	1.74	215
0.05	0.8	1507	1.72	92
		1362	1.82	1175
		1426	1.81	468
		1460	1.75	314
		1487	1.71	254
		1556	1.68	121
0.1	0.8	1413	1.74	1726
		1496	1.75	619
		1517	1.74	499
		1606	1.68	191
		1708	1.62	83
		1448	4.68	556
		1576	4.54	182
		1609	5.41	96
		1635	5.67	77
		1668	4.09	57
0.2	0.8	1726	5.22	35
		1517	1.70	1203
		1574	1.69	731
		1672	1.67	239
		1717	1.59	181
		1426	1.71	622
0.5	4.0	1466	1.69	400
		1534	1.68	179
		1552	1.62	162
1.0	8.0	1342	1.72	924
		1366	1.75	747
		1393	1.67	486
1.25	20	1473	1.56	198
		1310	1.85	318
		1392	1.81	109
Iso-octane				
0.01	0.125	1545	1.44	1966
		1592	1.42	1260
		1652	1.39	741
		1714	1.39	413
		1810	1.34	197
		1922	1.30	100
0.025	0.3125	2009	1.29	63
		1491	1.31	1954
		1495	1.50	1994
		1516	1.45	1648
		1564	1.47	940
		1601	1.44	689
		1647	1.46	406

Continued

Table I Continued

Fuel (%)	O ₂ (%)	T ₅ (K)	P ₅ (atm)	τ _{ign} (μs)
		1703	1.37	259
		1738	1.37	214
		1809	1.40	120
		1899	1.35	76
		1902	1.10	71
0.05	0.625	1455	1.45	1954
		1523	1.44	976
		1534	1.37	907
		1603	1.34	410
		1613	1.38	346
		1646	1.34	231
		1667	1.36	238
		1733	1.30	144
		1767	1.34	102
		1773	1.26	95
		1823	1.30	74
		1455	5.12	1290
		1484	7.50	767
		1521	4.89	576
		1618	6.88	199
		1672	4.74	141
		1699	6.51	96
		1800	4.48	52
0.1	1.25	1467	1.44	1454
		1480	1.47	1302
		1484	1.49	1334
		1543	1.49	651
		1551	1.42	573
		1642	1.30	269
		1642	1.38	227
		1823	1.33	68
0.125	6.25	1236	1.61	2700
		1337	1.55	756
		1394	1.52	345
		1476	1.43	130
		1598	1.40	47
0.25	3.125	1421	1.56	1576
		1487	1.46	758
		1598	1.42	223
		1646	1.35	147
		1763	1.37	64
0.25	6.25	1297	1.57	2370
		1361	1.50	1115
		1460	1.48	321
		1556	1.41	117
		1710	1.35	38
0.5	6.25	1318	1.53	2768
		1386	1.27	1365
		1393	1.48	1293
		1442	1.29	646
		1493	1.43	375
		1554	1.28	236
		1595	1.33	161
		1695	1.28	74

Continued

Table I Continued

Fuel (%)	O ₂ (%)	T ₅ (K)	P ₅ (atm)	τ _{ign} (μs)
		1700	1.18	66
		1766	1.26	51
		1206	5.53	2911
		1215	8.03	1621
		1251	7.69	1272
		1265	5.44	1624
		1305	5.33	1167
		1363	7.34	498
		1385	5.08	477
		1437	6.90	226
		1474	4.83	236
		1606	7.07	57
1.0	6.25	1360	1.44	2099
		1412	1.43	1170
		1512	1.46	486
		1589	1.35	199
		1177	8.17	2142
		1269	8.07	952
		1352	7.91	356
1.0	12.5	1238	1.46	1852
		1289	1.43	1248
		1302	1.32	1253
		1317	1.44	836
		1402	1.44	303
		1439	1.40	245
		1498	1.32	139
		1535	1.38	108
		1610	1.36	44

ignition time are the result of the regression analysis (see Fig. 3):

iso-butane (58 points):

$$\tau_{\text{ign}} = 6.90 \times 10^{-12} P^{-0.33} X_{\text{O}_2}^{-0.42} \Phi^{0.97} \times \exp(48560[\text{cal mol}^{-1}]/RT) \quad (1)$$

iso-pentane (34 points):

$$\tau_{\text{ign}} = 2.63 \times 10^{-12} P^{-0.59} X_{\text{O}_2}^{-0.61} \Phi^{1.30} \times \exp(49450[\text{cal mol}^{-1}]/RT) \quad (2)$$

iso-octane (95 points):

$$\tau_{\text{ign}} = 4.50 \times 10^{-10} P^{-0.56} \exp(-18.6 X_{\text{O}_2}) \Phi^{1.62} \times \exp(44780[\text{cal mol}^{-1}]/RT) \quad (3)$$

with ignition time τ_{ign} in s, pressure P in atm, oxygen mole fraction X_{O_2} , equivalence ratio Φ , activation energy E_A in cal mol^{-1} , and temperature T in K.

Note that the correlations for iso-butane and iso-pentane result in power law scaling for X_{O_2} , just as

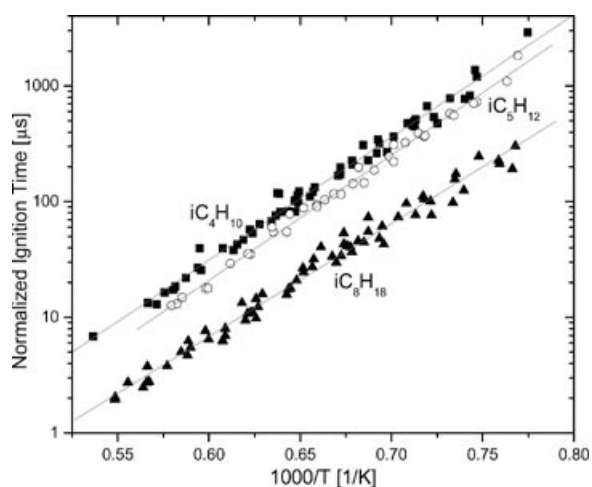


Figure 3 Correlated ignition times. All data normalized to 1 atm, $\Phi = 1$, and 21% O_2 . Filled squares, iso-butane; open circles, iso-pentane; filled triangles, iso-octane; lines, correlations.

the normal alkanes have shown [20], but iso-octane also has an exponential scaling with X_{O_2} . This exponential scaling results from a dramatic decrease in the iso-octane ignition time with O_2 mole fraction and is in agreement with previous high concentration data from Niemitz et al. [3] and Burcat et al. [1] and the trends predicted with detailed mechanisms [11–14]. For details on the dependence of iso-octane ignition times on T , P , Φ , and X_{O_2} see Davidson et al. [24].

No previous data were found, to allow comparisons with our iso-butane and iso-pentane data, though previous ignition time data do exist for iso-octane [1–4]. Our measurements agree best with the data of Niemitz et al. [3]; the data of Burcat et al. [1] appear to converge with our data at the upper end of their temperature range, while the data of Vermeer et al. [2] disagree dramatically (see Fig. 4). [The Vermeer et al. data were taken in a small square section shock tube, at very high fuel concentrations, using a photographic technique.] The highest quality shock tube data are obtained at low concentrations with short test times (< 1 ms). With higher fuel concentrations the pressure and temperature decrease after the shock arrival as the fuel undergoes endothermic thermal decomposition. With longer test times nonideal shock effects become of concern mainly as a result of the shock wave reflecting from the end-wall and traveling through a boundary layer created by the incident shock.

The ignition time data at 0.5% fuel concentration have been compared to seven models (Figs. 5–7). The iso-butane and iso-pentane models predict the experimental activation energy well, but there is disagreement between the measured and modeled activation energy

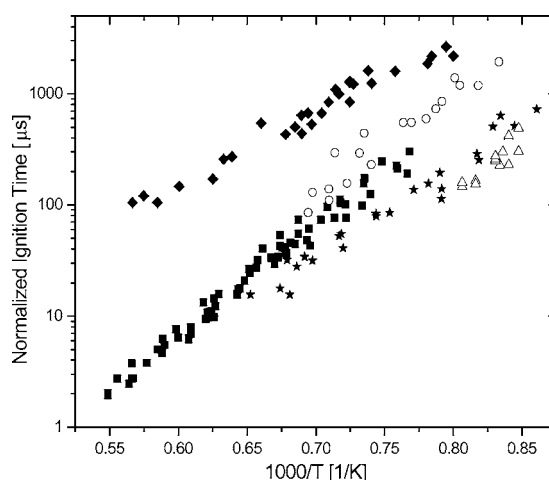


Figure 4 Correlated iso-octane ignition times: various shock tube studies. All data normalized to 1 atm, $\Phi = 1$, and 21% O_2 . Filled squares, current study; open circles, Niemitz et al. [3]; stars, Burcat et al. [1]; diamonds, Vermeer et al. [2]; open triangles, Nixon et al. [4].

for iso-octane. These models all predict the ignition time within a factor of two of our experiment. Current calculations have been carried out using CHEMKIN II with a constant volume constraint. The modeled ignition time was defined in the same manner as that of the experiment, by extrapolating the maximum slope of the CH concentration to the zero value.

Ignition times are useful parameters to assess the overall performance of a combustion chemistry model, but more detailed information about the transient radical pool is needed to further evaluate these

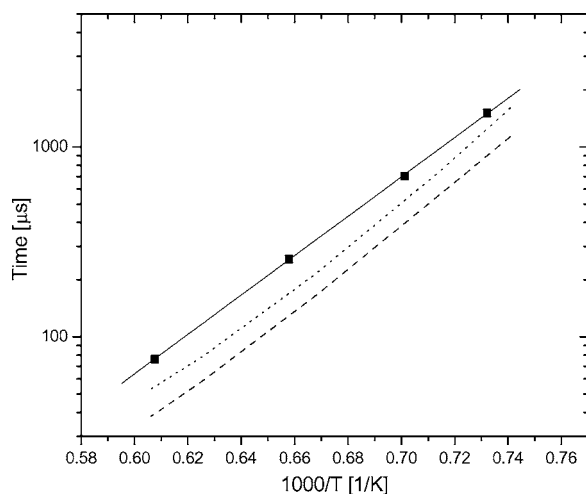


Figure 5 Variation of iso-butane ignition time with temperature: 0.5% iso-butane, 3.25% O_2 , $\Phi = 1$, 1.5 atm. Filled squares, current study; solid line, fit to data with $E_A = 47.4$ kcal mol $^{-1}$; dotted line, Bounaceur and Battin-Leclerc [6]; dashed line, Wang et al. [7].

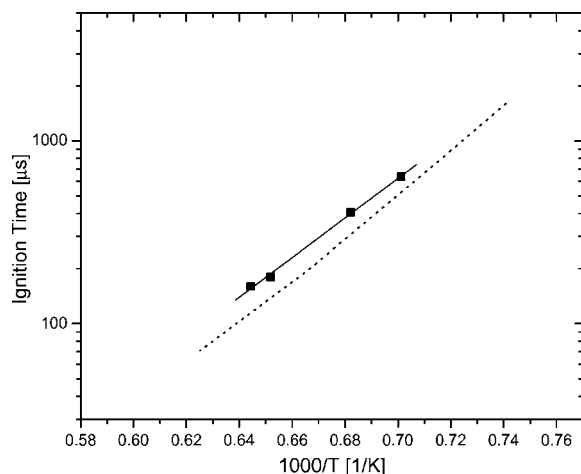


Figure 6 Variation of iso-pentane ignition time with temperature: 0.5% iso-butane, 4.0% O₂, $\Phi = 1$, 1.65 atm. Filled squares, current study; solid line, fit to data with $E_A = 49.4$ kcal mol⁻¹; dotted line, Bounaceur and Battin-Leclerc [6].

mechanisms. Information about the time history of the transient OH radical during branched alkane oxidation is presented in the next section.

OH Concentration Time Histories

The structure of the OH time history data is similar for the three different fuels. After shock heating, fuel decomposition liberates H-atoms which react with O₂

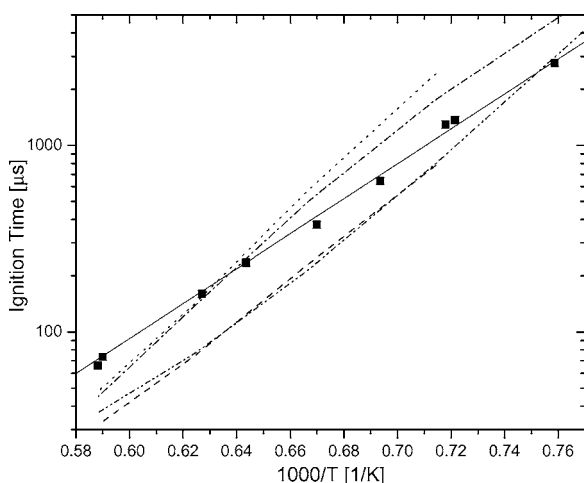


Figure 7 Variation of iso-octane ignition time with temperature: 0.5% iso-butane, 6.25% O₂, $\Phi = 1$, 1.3 atm. Filled squares, current study; solid line, fit to data with $E_A = 43.9$ kcal mol⁻¹; dashed line, Curran et al. [11]; dotted line, Davis and Law [12]; dot-dashed line, Ranzi et al. [14]; dot-dot-dashed line, Pitsch et al. [13].

to form OH; shortly thereafter, the OH concentration decreases to an intermediate minimum before ignition, where the OH concentrations rise rapidly. The structure of the OH concentration history during branched alkane oxidation is in stark contrast to previous work from our laboratory on *n*-alkane oxidation [17]. During *n*-alkane oxidation the OH rises to a plateau prior to ignition rather than declining to a minimum. The strong suppression of OH during branched alkane oxidation, particularly at the lowest temperatures of this study, is one indicator as to why branched alkanes inhibit knock in engine applications.

Example OH concentration data are shown in Fig. 8 for iso-butane. Table II summarizes the specific detail of the OH concentration time-history profiles. In this table, τ_1 (peak), τ_2 (min), and τ_3 (50%) are the times for the OH mole fraction to reach the first peak value, the minimum after this peak, and 50% of the second plateau level respectively; X(1st max), X(min), and X(2nd max) are the OH mole fraction initial peak, the minimum or plateau value, and the post-ignition peak value respectively. k_v is the absorption coefficient used to convert the measured absorbance to OH mole fraction via Beer's Law: $I/I_0 = \exp(-k_v P X_{OH} L)$. Model results indicate that τ_3 (50%) is nearly coincident with the maximum of the CH concentration (which is closely equivalent to the maximum rate of change of the CH endwall emission). The measured values of τ_3 (50%) are in good agreement with the simultaneously measured endwall ignition times if the small sidewall time correction of Petersen et al. [25] is applied. This correction (~ 10 – 40 μ s) is generally required for measurement of ignition time where the observation is made away from the endwall.

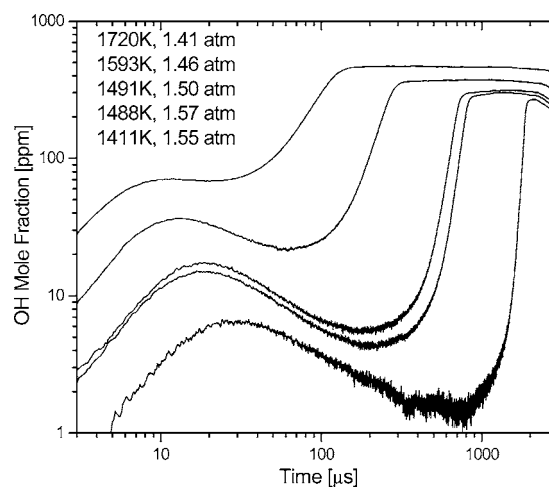


Figure 8 Iso-butane OH absorption data. Initial conditions: 0.1% iso-butane, 0.65% O₂. Upper trace 1720 K, lower trace 1411 K.

Table II Summary of OH Absorption Data

T_5 (K)	P_5 (atm)	k_v ($\text{atm}^{-1} \text{cm}^{-1}$)	τ_1 (peak)* (μs)	X (1st max) (ppm)	τ_2 (min)* (μs)	X (min) (ppm)	τ_3 (50%)* (μs)	X (2nd max) (ppm)
0.5% iso-butane, 3.25% O ₂								
1366	1.61	195	16	5	346	3	1429	Sat.
1426	1.55	184	9	13	198	6	680	Sat.
1520	1.49	167	7	34	76	17	233	Sat.
1646	1.46	145	4	96	20	63	65	Sat.
0.25% iso-butane, 3.25% O ₂								
1339	1.69	257	27	4	353	2	1128	641
1402	1.62	251	19	10	156	6	488	646
1488	1.58	232	11	28	55	19	165	777
1541	1.47	222	9	45	30	36	93	831
0.125% iso-butane, 3.25% O ₂								
1291	1.67	209	65	3	381	2	1476	342
1341	1.63	199	45	9	212	6	735	386
1390	1.56	191	34	19	130	15	372	466
1474	1.51	175	26	56	40	55	120	608
0.1% iso-butane, 0.65% O ₂								
1411	1.55	187	30	6	550	2	1810	268
1488	1.57	171	18	15	212	4	758	303
1491	1.50	172	19	17	178	6	662	315
1593	1.46	154	13	37	61	22	237	375
1720	1.41	135	12	71	20	69	87	470
0.05% iso-butane, 0.325% O ₂								
1444	1.59	179	33	7	390	2	1770	143
1546	1.58	164	23	17	155	7	572	177
1630	1.49	147	18	29	61	23	248	214
1703	1.40	138	18	42	31	41	146	242
1603	2.70	99	12	21	69	11	255	187
1625	2.50	131	12	23	55	14	224	187
1723	2.50	120	11	37	24	35	100	255
1545	5.61	54	7	9	85	3	368	137
1577	5.03	88	7	16	64	5	255	180
1750	4.78	81	5	42	12	40	49	254
0.5% iso-pentane, 4.0% O ₂								
1534	1.68	146	7	21	117	12	235	Sat.
1552	1.62	162	5	28	113	15	212	Sat.
0.1% iso-pentane, 0.8% O ₂								
1413	1.74	134	19	9	458	2	1788	344
1517	1.74	139	9	26	112	8	551	396
1606	1.68	145	7	44	44	19	219	459
1708	1.62	131	6	71	22	56	95	571
1609	5.40	83	3	18	17	4	183	281
1635	5.67	84	3	35	13	7	146	308
1726	5.22	81	2	39	10	19	103	355
1.0% iso-octane, 6.25% O ₂								
1322	1.58	206	3	12		1		Sat.
1398	1.43	192		31		1	1422	Sat.
1506	1.42	172		26		3	589	Sat.
1656	1.34	147		103	17	12	127	Sat.
0.5% iso-octane, 6.25% O ₂								
1330	1.55	205	4	17		4	1870	Sat.
1408	1.50	190	3	42		2	880	Sat.

Continued

Table II Continued

T_5 (K)	P_5 (atm)	k_v ($\text{atm}^{-1} \text{cm}^{-1}$)	τ_1 (peak)* (μs)	X (1st max) (ppm)	τ_2 (min)* (μs)	X (min) (ppm)	τ_3 (50%)* (μs)	X (2nd max) (ppm)
1507	1.43	154		100		7	280	Sat.
1641	1.37	148		149	12	34	62	Sat.
0.25% iso-octane, 6.25% O ₂								
1299	1.63	209	6	16		1	1825	Sat.
1394	1.53	198	4	49	49	2	621	Sat.
1467	1.48	178	3	93	14	12	226	Sat.
1570	1.41	160		159		42	62	Sat.
0.05% iso-octane, 0.625% O ₂								
1449	1.59	185	8	16		1	2182	245
1511	1.51	173	6	22		2	1152	288
1614	1.43	151	5	30	86	9	388	352
1736	1.40	132	5	44	27	36	137	456

Note: Sat. indicates transmission ~ 0 .

The predictions of the previously introduced models are shown in Figs. 9–11. These mechanisms all capture the general behavior of the OH concentration data although not the absolute OH yield. The two iso-butane models (Bounaceur and Battin-Leclerc, Wang et al.) capture the OH yield and ignition time within a factor of two. The Bounaceur and Battin-Leclerc mechanism captures the ignition time and the Wang et al. mechanism captures the early OH time history but not the absolute OH yield at early times. The Bounaceur and Battin-Leclerc iso-pentane mechanism does a fairly good job of predicting ignition but does not predict the early time rise followed by radical scavenging. The

iso-octane mechanisms all capture the general form of the OH profiles. The Ranzi et al. mechanism most closely captures the strong OH suppression and the Curran et al. and Ranzi et al. mechanism both do a good job of capturing the initial peak, capturing it to within a factor of two. The smaller Davis and Law and Pitsch et al. mechanisms both overpredict the initial peak and OH minimum, but the Davis and Law mechanism still captures the ignition time well.

Contribution and Sensitivity Analysis

Contribution and sensitivity analysis was performed on the Wang et al. and Bounaceur and Battin-Leclerc

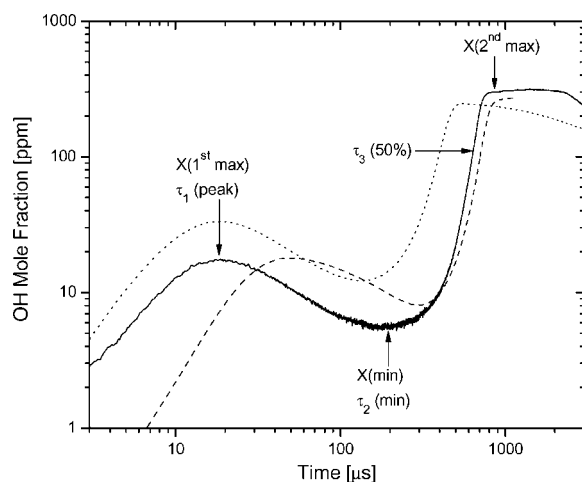


Figure 9 Iso-butane OH absorption data and comparison with models. Initial shock conditions: 0.1% iso-butane, 0.65% O₂, 1491 K, 1.50 atm. Solid line, measurement; dashed line, Bounaceur and Battin-Leclerc [6]; dotted line, Wang et al. [7].

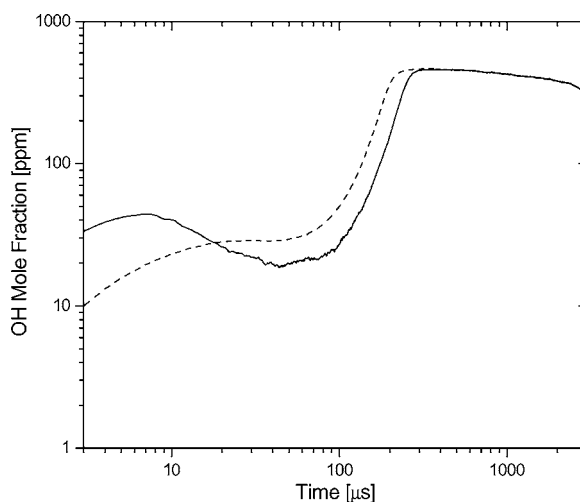


Figure 10 Iso-pentane OH absorption data and comparison with models. Initial shock conditions: 0.1% iso-pentane, 0.8% O₂, 1606 K, 1.68 atm. Solid line, measurement; dashed line, Bounaceur and Battin-Leclerc [6].

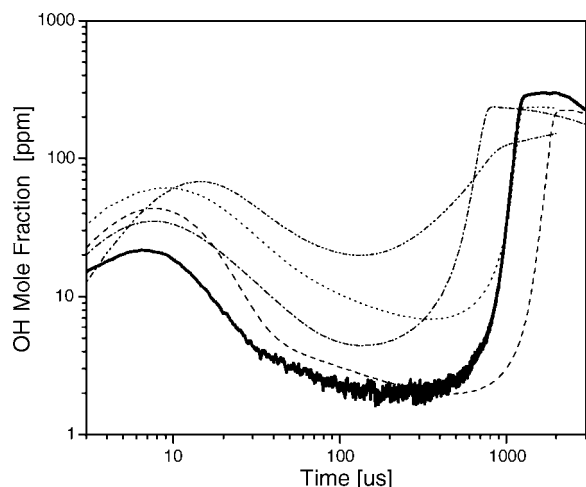


Figure 11 Iso-octane OH absorption data (corrected) and comparison with models. Initial shock conditions: 500 ppm iso-octane, 0.625% O₂, 1511 K, 1.51 atm. Solid line, measurement; dotted line, Davis and Law [12]; dashed line, Ranzi et al. [14]; dot-dashed line, Curran et al. [11]; dot-dot-dashed line, Pitsch et al. [13].

iso-butane mechanisms, the Bounaceur and Battin-Leclerc iso-pentane mechanism, and the Davis and Law iso-octane mechanism.

Contribution analysis shows that the early time rise in OH is due to fuel decomposition yielding alkyl radicals which in turn liberate H-atoms; H-atoms subsequently react with O₂ creating OH. The decrease in OH concentration (scavenging) results from OH reactions with olefins (H-atom abstraction) and reactions (mostly H-atom abstraction) with the other intermediates (CH₃, H₂, CH₂O, CO, and others). The ignition event is a result of the continued reaction of intermediates to a point at which enough radicals are present for chain branching to take over. At this point the OH concentration is almost entirely controlled by H + O₂.

In contrast to normal alkanes, branched alkanes exhibit radical scavenging with an intermediate pool that includes less H-atoms [1]. During intermediate to high temperature hydrocarbon oxidation, H-atoms are formed via: $RH + M \rightarrow R + H + M$ followed by beta-scission ($R + M \rightarrow \text{olefin} + H + M$). This reaction sequence is slower in branched isomers relative to normal isomers because the number of primary C-H bonds (stronger bonds) is greater in the case of the branched isomer. Therefore, production of methyl ($R + M \rightarrow \text{olefin} + CH_3 + M$) is more likely during branched alkane oxidation than during normal alkane oxidation. Once released, the methyl reacts with OH, acting as a scavenger.

Sensitivity analysis is presented for the Wang et al. iso-butane mechanism in Figs. 12 and 13.

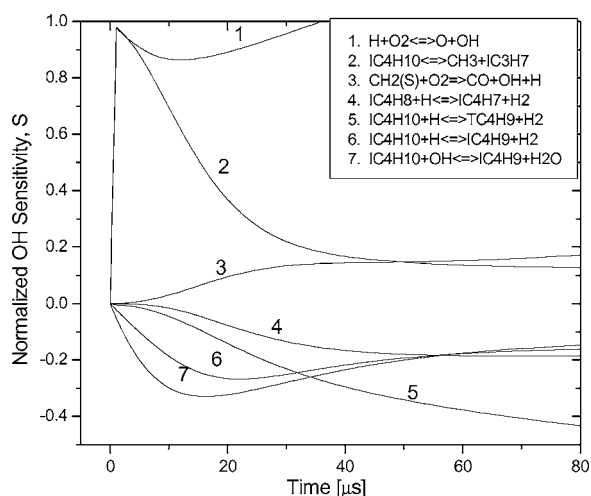


Figure 12 Early time OH sensitivity: Iso-butane. 0.1% iso-butane, 0.65% O₂, 1491 K, 1.5 atm. $S = d[OH]/dk_i (k_i/[OH]_{\text{local}})$.

The other mechanisms show similar sensitivity. Sensitivity is defined for our purposes here as $S = (d[OH]/dk_i)(k_i/[OH]_{\text{local}})$. Sensitivity analysis shows that at early times (Fig. 12), prior to scavenging, the OH yield is sensitive to $H + O_2 \rightarrow O + OH$ and fuel decomposition reactions. The scavenging of OH, providing the plateau, is sensitive to: fuel + H, fuel + OH, and olefin + H. The analysis shows that the fate of OH during the induction period is sensitive to the rates of decomposition and H-atom abstraction reactions. A more complete inclusion of these reactions and improvements to the rate coefficients will provide better modeling of the OH yield during the initial rise and

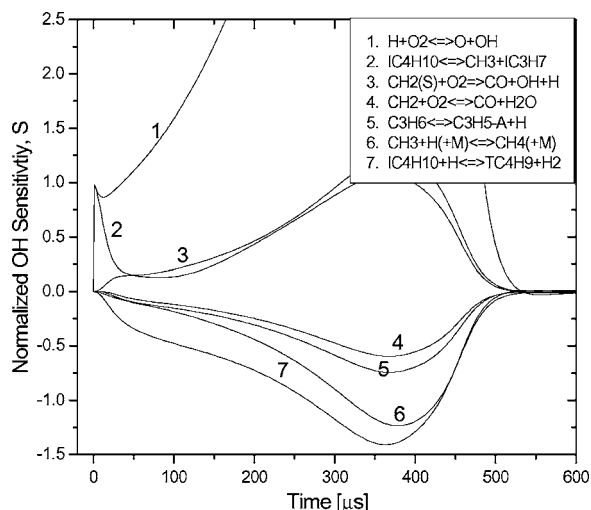


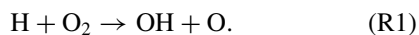
Figure 13 Longer time OH sensitivity: Iso-butane. 0.1% iso-butane, 0.65% O₂, 1491 K, 1.5 atm. $S = d[OH]/dk_i (k_i/[OH]_{\text{local}})$.

scavenging periods. The OH yield during the ignition event is strongly sensitive to $\text{H} + \text{O}_2$ as well as $\text{CH}_2 + \text{O}_2$, $\text{CH}_2(\text{S}) + \text{O}_2$, fuel decomposition, fuel + H, and other intermediate decomposition reactions.

Published high temperature values for the branched alkane decomposition reaction rates are scarce and vary greatly [26], as is also the case for the normal alkanes. Improved values for these reaction rates are needed if the small radical pool is to be accurately predicted in these shock tube experiments and other high temperature combustion environments.

OH rise times and initial plateau levels are strongly sensitive to the formation rate of H-atoms from fuel decomposition reactions and their subsequent reaction with O_2 . Some estimate of these decomposition rates can be obtained from this early time OH data, though this has not been done here, because of the uncertainties associated with other H-atom and OH reactions (fuel + H, fuel + OH, and $\text{CH}_2(\text{S}) + \text{O}_2 \rightarrow \text{OH} + \text{CO} + \text{H}$). However, measurements of CH_3 concentration profiles would offer a more direct measurement of these fuel decomposition reactions, and experiments to measure CH_3 in these systems, using narrow-linewidth laser absorption at 216 nm, are currently under development.

The entire OH concentration time history shows very strong sensitivity to:



Confidence in this rate coefficient has improved over the years and recent publications [27–30] put an uncertainty of only 9% on this rate over the temperature range 1336–3370 K [27]. Despite the extensive efforts made to refine this rate, some of the mechanisms still use the older rate coefficient recommended by Baluch et al. [31] in 1992. This rate varies by up to 30% over portions of the temperature range from the Yu et al. [27] value published in 1994. Recent transition state calculations [32] published in 1997 also agree more closely with the Yu et al. value for k_1 . Simply changing k_1 in these mechanisms to the Yu et al. value provides an improvement in terms of modeling our data. Figure 14 shows the result of changing the rate coefficient in the Wang et al. mechanism from $k_1 = 1.97 \times 10^{14} \exp(-8324/T) \text{ cm}^3 \text{ mol}^{-1} \text{ s}^{-1}$ (Baluch et al.) to $k_1 = 8.3 \times 10^{13} \exp(-7253/T) \text{ cm}^3 \text{ mol}^{-1} \text{ s}^{-1}$ (Yu et al.). Notice that changing the rate coefficient shifts the modeled predictions of OH downward towards the data, improving the predictions.

The next step in improvement of these and future mechanisms lies in several areas: (1) adjustment of critical rate coefficients in a systematic manner within

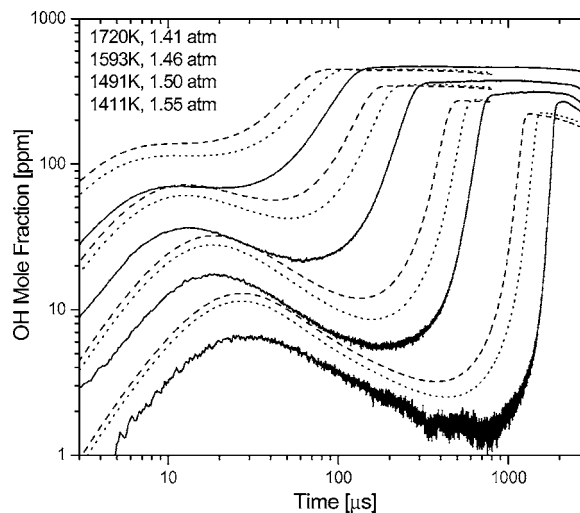


Figure 14 Iso-butane OH absorption data and comparison with models. Initial conditions: 0.1% iso-butane, 0.65% O_2 . Upper traces 1720 K, lower traces 1411 K. Solid line, this study; dashed line, Wang et al. with $k_1 = 1.97 \times 10^{14} \exp(-8324/T) \text{ cm}^3 \text{ mol}^{-1} \text{ s}^{-1}$; dotted line, Wang et al. with $k_1 = 8.3 \times 10^{13} \exp(-7253/T) \text{ cm}^3 \text{ mol}^{-1} \text{ s}^{-1}$.

their uncertainty limits; (2) direct and improved measurement of the most important rate coefficients; (3) continued generation of target data for model constraint (i.e., larger range of conditions, additional species, and parameters); and (4) experimental and computational work on important olefin species which are of importance as intermediates during intermediate to high temperature alkane oxidation.

CONCLUSIONS

A database of ignition times and OH concentration time histories has been generated for three branched alkanes: iso-butane, iso-pentane, and iso-octane. A comparison of several current models with our ignition time data showed that the models perform reasonably well, though there is considerable room for improvement. The iso-butane and iso-pentane models do an excellent job of capturing the temperature dependence of the ignition time and predict the ignition time to within a factor of two. The iso-octane models do a reasonable job at predicting the ignition time (factor of two) but do not capture the temperature dependence. Comparison of the measured OH data with the models shows varying results; this is to be expected as none of these models has been validated or optimized using transient radical pool data. Researchers involved in creation of mechanisms for the modeling of branched alkane oxidation should find these data useful in the refining of their models.

BIBLIOGRAPHY

- Burcat, A.; Pitz, W. J.; Westbrook, C. K. 18th Intl Symp Shock Waves 1991, 771–780.
- Vermeer, D. J.; Meyer, J. W.; Oppenheim, A. K. Combust Flame 1972, 18, 327–336.
- Niemitz, K. J.; Zellner, R.; Essner, C.; Warnatz, J. data reproduced in Westbrook, C. K.; Warnatz, J.; Pitz, W. J. Proc Comb Inst 1998, 22, 893–901.
- Nixon, A. C.; Ackerman, G. H.; Hawthorn, R. D.; Henderson, H. T.; Ritchie, A. W. Technical Documentary Report No. APL-TDR-64-100 Part II, Air Force Aero Propulsion Laboratory Wright-Paterson AFB 1966.
- Fiewieger, K.; Blumenthal, R.; Adomeit, G. Combust Flame 1997, 109, 599–619.
- Bounaceur, R.; Battin-Leclerc, F. Private communication 2002, EXGAS: Automatic generation of detailed and reduced mechanism. Available from Département de Chimie-Physique des Réactions INPL-ENSIC-Nancy: <http://www.ensic.inpl-nancy.fr/ENSIC/DCPR/Anglais/GCR/softwaredescription/exgas.htm>.
- Wang, S.; Miller, D. L.; Cernansky, P.; Curran, H. J.; Pitz, W. J.; Westbrook, C. K. Combust Flame 1999, 118, 415–430.
- Battin-Leclerc, F.; Glaude, P. A.; Warth, V.; Fournet, R.; Scacchi, G.; Côme, G. M. Chem Eng Sci 2000, 55, 2883–2893.
- Côme, G. M.; Warth, V.; Glaude, P. A.; Fournet, R.; Battin-Leclerc, F.; Scacchi, G. Proc Comb Inst 1997, 27, 755–762.
- Barbé, P.; Battin-Leclerc, F.; Côme, G. M. J Chem Phys 1995, 92, 1666–1692.
- Curran, H. J.; Pitz, W. J.; Westbrook, C. K.; Callahan, C. V.; Dryer, F. L. Proc Comb Inst 1998, 27, 379–387.
- Davis, S. G.; Law, C. K. Proc Comb Inst 1998, 27, 521–527.
- Pitsch, H.; Peters, N.; Seshadri, K. Proc Comb Inst 1996, 26, 763–771; and private communications with H. Pitsch.
- Ranzi, E.; Faravelli, T.; Gaffuri, P.; Sogaro, A.; D'Anna, A.; Ciajolo, A. Combust Flame 1997, 108, 24–42.
- Held, T. J.; Marchese, A. J.; Dryer, F. L. Combust Sci Technol 1997, 123, 107–146.
- Ranzi, E.; Gaffuri, P.; Faravelli, T.; Dagaut, P. Combust Flame 1995, 103, 91–106.
- Davidson, D. F.; Herbon, J. T.; Horning, D. C.; Hanson, R. K. Int J Chem Kinet 2001, 33, 775–783.
- Horning, D. C.; Davidson, D. F.; Hanson, R. K. 23rd Intl Symp Shock Waves 2001, Paper No. 5731.
- Burcat, A.; McBride, B. Ideal Gas Thermodynamic Data for Combustion and Air-Pollution Use; Technion Aerospace Engineering (TAE), 1997; Report No. 804.
- Horning, D. C.; Davidson, D. F.; Hanson, R. K. J Propulsion Power 2002, 18, 363–371.
- Wooldridge, M. S.; Hanson, R. K.; Bowman, C. T. Int J Chem Kinet 1994, 26, 389–401.
- Herbon, J. T.; Hanson, R. K.; Golden, D. M.; Bowman, C. T. Proc Comb Inst 2002, 29, 1201–1208.
- Davidson, D. F.; Horning, D. C.; Herbon, J. T.; Hanson, R. K. Proc Comb Inst 2000, 28, 1687–1692.
- Davidson, D. F.; Oehlschlaeger, M. A.; Herbon, J. T.; Hanson, R. K. Proc Comb Inst 2002, 29, 1295–1301.
- Petersen, E. L.; Davidson, D. F.; Hanson, R. K. J Propulsion Power 1999, 15, 82–91.
- NIST Chemical Kinetics Database 2000, Standard Reference Database 17, Version 7.0.
- Yu, C.-L.; Frenklach, M.; Masten, D. A.; Hanson, R. K.; Bowman, C. T. J Phys Chem 1994, 98, 4470–4471.
- Hong, D.; Hessler, J. P. J Chem Phys 1992, 96, 1077–1092.
- Shin, K. S.; Michael, J. V. J Chem Phys 1991, 95, 262–273.
- Masten, D. A.; Hanson, R. K.; Bowman, C. T. J Phys Chem 1990, 94, 7119–7128.
- Baulch, D. L.; Cobos, C. J.; Cox, R. A.; Esser, C.; Frank, P.; Just, Th.; Kerr, J. A.; Pilling, M. J.; Troe, J.; Walker, R. W.; Warnatz, J. J Phys Chem Ref Data 1992, 21, 411–429.
- Miller, J. A.; Garrett, B. C. Int J Chem Kinet 1997, 29, 275–287.